Pakistan Veterinary Journal

ISSN: 0253-8318 (PRINT), 2074-7764 (ONLINE)
DOI: 10.29261/pakvetj/2025.335

RESEARCH ARTICLE

# Quercetin Ameliorates Cognitive Impairment in App/Ps1 Mice Via Gut Microbiota Modulation and Tryptophan Metabolism Restoration

Ying Feng[1†], Yan hua Shi[2†], Tao Wang[3], Jin yang Han[1], Dan dan Li[1], Xiao tong Zhang[1], Qian Xu[1], Feng Liu[4], Jingjing Wei[4] and Xinjun Yu[1]*

[1]Affiliated Hospital of Shandong Second Medical University, Weifang, China; [2]College of Life Science and Technology, Shandong Second Medical University, Weifang, China; [3]School of Clinical Medicine, Affiliated Hospital of Shandong Second Medical University, Weifang, China: [4]College of Veterinary Medicine, Northwest A&F University, 712100 Yangling, China. †These authors contributed equally to this work.
*Corresponding author: fyyuxj@sdsmu.edu.cn

ARTICLE HISTORY (25-957)

Received: October 06, 2025
Revised: December 12, 2025
Accepted: December 18, 2025
Published online: December 20, 2025

**Key words:**
Gut-brain axis
Indole-3-propionic acid
Neurodegenerative disease
Quercetin
Tryptophan metabolism

**ABSTRACT**

Emerging evidence positions the bidirectional microbiome-brain communication network as a tractable intervention point in neurodegeneration. Yet whether dietary flavonoids can leverage this axis to counteract cognitive decline remains incompletely characterized. Three cohorts of male APP/PS1 mice underwent daily oral administration of quercetin (100mg/kg body weight) or saline vehicle over a 6-month intervention period. Spatial learning and memory were evaluated through Morris Water Maze paradigms. Multi-omics profiling encompassed fecal microbiome characterization (16S rRNA gene amplicon sequencing), serum metabolomic analysis (liquid chromatography-tandem mass spectrometry), and hippocampal transcriptome mapping (RNA sequencing). Relative to vehicle-treated APP/PS1 controls, quercetin intervention elicited marked improvements across multiple spatial memory indices. Specifically, treated animals demonstrated enhanced target quadrant exploration (swimming distance: 11±2m versus 9±2.5m in controls; $P<0.001$) and prolonged occupancy within the goal zone (12.3±2.2s compared to 7.5±2.2s; $P<0.001$). Platform crossing frequency nearly doubled following quercetin administration (4.4±0.6 versus 2.1±0.6 crossings; $P<0.01$), while acquisition-phase escape latency on day 5 decreased by 23% (30s versus 39s in untreated mice). These behavioral improvements coincided with substantial gut microbiome restructuring, characterized by a 3.6-fold reduction in pathogenic Escherichia-Shigella abundance ($log_2$fold-change = -1.83; $P<0.001$). Concurrently, circulating tryptophan concentrations rose by 26% (from 380±86 to 480±88ng/mL; $P<0.01$), while its microbial-derived metabolite indole-3-propionic acid exhibited an 89% increase (579±99ng/mL in controls versus 1098±83ng/mL post-treatment; $P<0.001$). Transcriptomic interrogation of brain tissue identified significant enrichment of aryl hydrocarbon receptor signaling. Our findings demonstrate that quercetin counteracts Alzheimer's-associated cognitive impairment via coordinated restoration of intestinal microbial ecology and tryptophan catabolic pathways, with aryl hydrocarbon receptor activation potentially serving as a downstream neuroprotective effector mechanism.

**To Cite This Article:** Feng Y, Shi YH, Wang T, Han JY, Li D, Zhang XT, Xu Q, Liu F, Wei J and Yu X, 2025. Quercetin ameliorates cognitive impairment in app/ps1 mice via gut microbiota modulation and tryptophan metabolism restoration. Pak Vet J, 45(4): 1698-1709. http://dx.doi.org/10.29261/pakvetj/2025.335

## INTRODUCTION

Neurodegenerative diseases (NDs) affect both humans and companion animals, causing progressive cognitive decline (Story *et al.*, 2020; Dewey, 2025). Alzheimer's disease (AD), the most prevalent neurodegenerative disorder, affects over 55 million individuals globally, with projections indicating this number will triple by 2050, imposing substantial socioeconomic burdens on healthcare systems worldwide. Current treatments show limited efficacy and often carry significant side effects (Metwally *et al.*, 2023). Despite decades of intensive research and substantial

investment in drug development, the failure rate of AD clinical trials exceeds 99%, with most amyloid-β-targeting therapies demonstrating minimal clinical benefit. This therapeutic impasse underscores the urgent need for alternative intervention strategies that address the multifactorial nature of neurodegeneration. The pathogenesis involves protein misfolding, neuroinflammation, and mitochondrial dysfunction (Wihadmadyatami *et al.*, 2025). Recent studies have focused on the microbiota-gut-brain axis as a potential regulatory pathway in ND progression (Sampson *et al.*, 2016; Cryan *et al.*, 2019).

Gut microbiota dysbiosis has been observed in ND patients and animal models, with microbial changes correlating with cognitive impairment (Vogt *et al.*, 2017). Specifically, AD patients exhibit reduced microbial diversity, altered Firmicutes-to-Bacteroidetes ratios, and expansion of pro-inflammatory bacterial taxa, suggesting that intestinal microbial imbalance may precede or exacerbate neurological pathology. However, the precise mechanisms linking gut dysbiosis to cognitive decline remain poorly defined, limiting the development of microbiota-targeted therapeutic interventions. Among microbial metabolites, tryptophan (TRP) derivatives play important roles in neuroimmune regulation (Agus *et al.*, 2018). ndole-3-propionic acid (IPA), a bacterial metabolite of dietary tryptophan, acts as an aryl hydrocarbon receptor (AhR) agonist and shows neuroprotective effects (Rothhammer and Quintana, 2019). Studies have shown that IPA reduces neuroinflammation and amyloid-β (Aβ) accumulation in Alzheimer's disease models (Rothhammer *et al.*, 2018; Sun *et al.*, 2022). However, how gut microbial imbalances affect TRP metabolism in NDs is not fully understood. Furthermore, whether restoration of microbial tryptophan metabolism can reverse established cognitive deficits, and which specific bacterial taxa are responsible for IPA production in the context of neurodegeneration, remain critical unanswered questions.

Quercetin, a dietary flavonoid, possesses antioxidant and anti-inflammatory activities with potential neuroprotective benefits (Lu *et al.*, 2017). Emerging evidence indicates quercetin modulates gut microbiota composition, initially observed in metabolic disease research (Porras *et al.*, 2017; Liu *et al.*, 2025). Lv found that quercetin improves cognitive function and reduces Aβ and tau pathology in APP/PS1 mice, partly by restoring gut microbial diversity (Lv *et al.*, 2018). However, these previous studies primarily focused on taxonomic shifts without mechanistic investigation of metabolic pathways. But whether quercetin's effects in NDI depend on gut microbiota-mediated TRP metabolism remains unclear.

In this study, we employed APP/PS1 transgenic mice to evaluate quercetin's impact on cognitive performance. Multi-omics approaches characterized quercetin-induced changes in gut microbiota, systemic tryptophan metabolism, and associated signaling cascades. These findings support the microbiota-gut-brain axis as a promising therapeutic strategy for neurodegenerative disorders.

## MATERIALS AND METHODS

**Animal experiments:** The Alzheimer's disease model consisted of male APPswe/PSEN1dE9 (APP/PS1) double transgenic mice (Jankowsky *et al.*, 2004). Male C57BL/6 mice of identical age were used as controls. Both strains were obtained from Nanjing Zhi Mouse Research & Biotechnology Co., Ltd. (Jiangsu, China). Mice were housed at 22±2°C with 60±5% humidity under a 12-hour light/dark cycle. Standard chow and water were provided ad libitum. The Institutional Animal Care and Use Committee of University approved this study (approval number: 2023-WFMC-DW-001).

Sample size determination employed power calculations with type I error set at 0.05, type II error at 0.2, and projected effect size of 1.2, yielding a minimum requirement of 10 mice per experimental arm. Upon reaching 3 months of age, APP/PS1 transgenic mice underwent block randomization into two arms: vehicle-treated disease controls (NDI, n=10) and quercetin intervention group (n=10). Age-matched wild-type C57BL/6 littermates (n=10) served as non-transgenic references. Pharmaceutical-grade quercetin (purity ≥98%; Sigma-Aldrich, Cat# Q4951) was freshly suspended in sterile 0.9% saline immediately before each administration and delivered via oral gavage at 100mg/kg daily. Disease control and wild-type cohorts received volume-matched saline vehicle. Blinded experimental design was maintained throughout: personnel performing behavioral assessments and biochemical quantifications remained naive to group allocation until statistical analysis completion. The intervention spanned 6 consecutive months, after which animals sequentially underwent cognitive testing and tissue collection for molecular profiling.

**Morris Water Maze (MWM):** Spatial learning and memory were evaluated using the Morris Water Maze paradigm (Morris, 1984). The apparatus comprised a circular tank (diameter 1.2m, height 0.35m) filled with water maintained at 22-24°C. A transparent escape platform (10cm diameter) was positioned 1cm beneath the water surface to remain visually undetectable. The testing protocol encompassed a 5-day acquisition phase (days 1-5) followed by a single probe trial on day 6. During acquisition, mice completed four trials daily. Each trial began from one of four pseudo-randomized starting points, with mice facing the pool wall. Mice had 60 seconds to locate the platform; those unsuccessful were manually guided to it. All mice stayed on the platform for 15 seconds for spatial consolidation. Escape latency measured the time from release to platform arrival (Vorhees and Williams, 2006). The probe trial on day 6 removed the platform to test memory retention. ANY-Maze software (version 6.2, Stoelting Co., Wood Dale, IL, USA) tracked movements. The Morris water maze protocol was optimized for transgenic AD mouse models following established guidelines for detecting spatial memory deficits (Bromley-Brits *et al.*, 2011). Analysis included: swimming distance in the target quadrant, time spent in the target quadrant, and platform location crossings.

**Gut microbiota profiling:** Fecal samples underwent 16S rRNA gene sequencing. The QIAamp PowerFecal Pro DNA Kit (Qiagen, catalog 51804) extracted genomic DNA. DNA purity was assessed using a NanoDrop 2000 spectrophotometer (Thermo Fisher Scientific, Waltham,

MA, USA). Samples showing A260/A280 ratios between 1.8 and 2.0 proceeded to library construction.

The V4 hypervariable region was amplified using primers 338F (5'-ACTCCTACGGGAGGCAGC-3') and 806R (5'-GGACTACHVGGGTWTCTAAT-3'). PCR conditions included initial denaturation at 95°C for 3 min, 27 cycles (95°C/30s, 55°C/30s, 72°C/45s), and final extension at 72°C for 10 min. We purified amplicons with MPure XP beads (Beckman Coulter, Brea, CA, USA) and quantified them using Qubit 4.0 fluorometry (Thermo Fisher Scientific). Paired-end sequencing (2×250 bp) was performed on an Illumina NovaSeq 6000 platform at Magi Gene Technology (Guangzhou, China).

QIIME2 (v2022.2) with DADA2 processed raw data (Callahan *et al*., 2016; Bolyen *et al*., 2019). Reads were truncated at 240bp (forward) and 220bp (reverse); sequences with >2.0 expected errors were discarded. SILVA database (release 138) classified ASVs at 0.7 confidence (Callahan *et al.*, 2016; Bolyen *et al.*, 2019). The SILVA ribosomal RNA gene database provides comprehensive quality-checked and aligned sequences for all three domains of life (Quast *et al.*, 2013). Sequencing yielded 52,347±3,215 reads/sample (range: 47,832-58,914). Good's coverage was >99.2%. Reads were rarefied to 45,000/sample. R (v4.2.1) conducted ecological analyses. Vegan package (v2.6-4) computed alpha diversity and PCoA plots (Quast *et al*., 2013). Microeco package (v0.20.0) performed LEfSe analysis to detect discriminatory taxa (Quast *et al.*, 2013; McMillan *et al.*, 2020).

**Metabolomics:** Serum samples stored at -80°C were extracted by mixing 50µL serum with 200µL ice-cold methanol containing L-phenylalanine-d5 (1µg/mL, internal standard). After vortexing (30s) and incubation (-20°C, 20 min), samples were centrifuged (13,000rpm, 15 min, 4°C). Supernatants were collected for analysis. Pooled QC samples ran every 10 injections to monitor system stability (Dunn *et al.*, 2011).

A Vanquish UHPLC coupled to an Orbitrap Exploris 120 (Thermo Fisher Scientific) performed metabolomic profiling. Separation used a Waters ACQUITY UPLC HSS T3 column (2.1×100mm, 1.8µm) at 40°C with 0.3mL/min flow. Mobile phases: 0.1% formic acid in water (A) and acetonitrile (B). Gradient: 0-1 min, 5% B; 1-9 min, 5-95% B; 9-11 min, 95% B; 11.1-14 min, 5% B. Injection volume: 2 µL. Data-dependent acquisition operated in both ESI modes with 4s dynamic exclusion. Source parameters: spray voltage 3.5kV (positive)/2.8kV (negative), sheath gas 40 units, auxiliary gas 10 units, capillary temperature 320°C. Full MS and MS/MS resolutions were 60,000 and 15,000, respectively; collision energies ranged 20-40eV. ProteoWizard (v3.0.21206) converted raw data to mzXML. XCMS (v3.18.0) detected features: peak width 10-60 s, mass tolerance 10 ppm, minimum difference 0.01 Da (Smith *et al.*, 2006). Metabolites were annotated by matching accurate mass (±5 ppm), MS/MS spectra, and retention times to HMDB (v5.0), METLIN, and proprietary databases. Features with QC CV >30% were removed. Quality control procedures followed standardized protocols for large-scale metabolomic studies to ensure data reliability and reproducibility (Dunn *et al.*, 2011). Missing values (present in >80% samples/group) underwent k-nearest neighbors imputation (k=5) and probabilistic quotient normalization. Metware Biotechnology (Wuhan, China) provided services. MetaboAnalyst (v4.0) performed pathway enrichment (Chong *et al.*, 2019).

**Proteomics:** Brain tissues stored at -80°C were lysed in 8M urea buffer with 1% protease inhibitor cocktail. BCA assay determined protein concentrations. Samples (100µg protein) were reduced with 5mM dithiothreitol (56°C, 30 min) and alkylated with 11mM iodoacetamide (room temperature, 15 min, dark). Overnight trypsin digestion occurred at 37°C (1:50 enzyme-to-substrate ratio, w/w) (Wiśniewski *et al.*, 2009). C18 cartridges desalted peptides, which were then vacuum-dried. A Vanquish UHPLC coupled to an Orbitrap Exploris 120 (Thermo Fisher Scientific, Waltham, MA, USA) separated peptides on a reversed-phase column (75µm i.d. × 25cm, 1.9µm C18) at 300nL/min. The 90-min gradient ramped from 5 to 35% acetonitrile in 0.1% formic acid. Full MS scans (m/z 350-1800) ran at 60,000 resolution (at m/z 200). The top 20 precursors underwent HCD fragmentation (28% collision energy); MS/MS spectra were acquired at 15,000 resolution. Dynamic exclusion: 30s.

MaxQuant (v2.0.3.0) searched spectra against mouse UniProt (Cox and Mann, 2008). Parameters: trypsin specificity, ≤2 missed cleavages; carbamidomethyl cysteine (fixed); oxidized methionine and N-terminal acetylation (variable); precursor tolerance 4.5ppm; fragment tolerance 20ppm. Match-between-runs enabled improved quantification (Tyanova *et al.*, 2016). Label-free quantification was performed using the MaxLFQ algorithm, which employs delayed normalization and maximal peptide ratio extraction to achieve accurate protein abundance measurements across samples (Cox *et al.*, 2014). Proteins required ≥2 unique peptides at 1% FDR. Perseus (v1.6.15.0) analyzed and visualized differential expression.

**UID RNA sequencing of brain tissue:** TRIzol reagent (Invitrogen, Cat# 15596026) extracted total RNA from approximately 50 mg brain tissue. An Agilent 2100 Bioanalyzer assessed RNA quality; samples with integrity numbers ≥7.5 proceeded to library construction. A Qubit 4.0 fluorometer determined RNA concentrations. Oligo (dT) magnetic beads captured polyadenylated transcripts, which were then fragmented to ~250 nucleotides (Badawy 2017). The dUTP method enabled strand-specific cDNA synthesis. Libraries underwent end-repair, adapter ligation, and 12-cycle amplification before paired-end sequencing (2×150bp) on an Illumina NovaSeq 6000 (Seqhealth Technology, Wuhan, China). Each sample generated 25.3±2.1 million clean reads on average. Fastp (v0.23.2) filtered raw data, retaining sequences with Q20 >95%. HISAT2 (v2.2.1) mapped reads to the mouse genome (GRCm39/mm39), achieving 94.2±1.8% alignment. Feature Counts (v2.0.3) quantified gene expression using GENCODE M30 annotations. DESeq2 (v1.36.0) identified differentially expressed genes (DEGs) with thresholds: $|\log_2 FC| > 0.58$ and Benjamini-Hochberg adjusted $p < 0.05$ (Love *et al.*, 2014). DESeq2 employs a negative binomial generalized linear model to account for biological variability and uses shrinkage estimation for dispersions

and fold changes, providing robust differential expression analysis for RNA-seq (Anders and Huber, 2010). Cluster Profiler (v4.4.4) performed Gene Set Enrichment Analysis against MSigDB Hallmark collections (Yu *et al.*, 2012). Pre-ranked gene lists underwent 1,000 permutations, with pathways considered enriched at FDR <0.25.

**Quantitative Analysis of Tryptophan and indole-3-propionic acid:** Serum samples (30µL) were mixed with 870µL ice-cold methanol containing L-tryptophan-d5 (500ng/mL, internal standard). Following incubation (-20°C, 20 min), samples were centrifuged (13,000rpm, 10 min, 4°C). Supernatants passed through 0.22µm filters before analysis. A Waters Alliance e2695 HPLC with Agilent ZORBAX XDB C18 column (30°C) separated analytes. Mobile phases: 0.1% formic acid in water (A) and acetonitrile (B) at 1.0mL/min. Fluorescence detection employed 280/348 nm (excitation/emission) for tryptophan and 270/390nm for indole-3-propionic acid. Calibration curves from authentic standards (10-5000ng/mL) showed excellent linearity ($r^2 > 0.999$). Intra-day precision was <12%; extraction recovery ranged 92-108%.

**Statistical analysis:** GraphPad Prism (v9.3.1, La Jolla, CA, USA) and R (v4.2.1) conducted statistical analyses. Data are shown as mean ± SD. The Shapiro-Wilk test checked normality. Normal data underwent one-way ANOVA with Dunnett's test (treatment vs. control) or Tukey's HSD (pairwise comparisons). Non-normal data were analyzed by Kruskal-Wallis test with Dunn's post-hoc. Pearson's correlation evaluated linear relationships; Spearman's correlation assessed monotonic associations. The Benjamini-Hochberg procedure controlled FDR in multi-omics datasets. Significance: P<0.05 or FDR <0.05 (specified in legends).

## RESULTS

**Quercetin ameliorated cognitive impairment in NDI mice:** As outlined in the experimental design (Fig. 1A), we evaluated cognitive function using the Morris Water Maze. Tracking analysis showed that NDI mice swam randomly, whereas quercetin-treated animals displayed a focused search strategy similar to controls (Fig. 1B). Quantitative analysis confirmed that quercetin significantly reversed NDI-induced deficits. While NDI mice spent less time (7.5±2.2s) and covered less distance (9±2.5m) in the target quadrant compared to controls, quercetin treatment restored these parameters to 12.3±2.2s and 11±2m, respectively (P<0.001; Fig. 1C-D). Furthermore, quercetin increased platform crossings (*4.4±0.6 vs. 2.1±0.6,* P<0.01; Fig. 1E) and improved learning efficiency, reducing Day 5 escape latency by 23% (30s vs. 39s; Fig. 1F).

(A) Experimental timeline. (B) Representative swimming trajectories during MWM probe trial across three groups (n=10/group). (C-F) MWM performance metrics: (C) total swimming distance, (D) duration in target quadrant, (E) platform crossings, (F) escape latency during acquisition phase. **P<0.01, ***P<0.001, ns=not significant (*one-way ANOVA with Tukey's post-hoc test*).

**Association between cognitive impairment and gut microbiota in NDI mice:** Accumulating evidence indicates that dysbiosis of the intestinal microbiota plays a critical role in the onset and progression of neurodegenerative diseases (NDs) (Abou Izzeddine *et al.*, 2025). Specifically, reduced microbial gene richness and altered Bacteroidetes abundance have been consistently associated with AD progression in clinical cohorts (Jung *et al.*, 2022).

To characterize intestinal bacterial community shifts, we subjected fecal samples from NDI mice to 16S rRNA gene sequencing. Chao1 estimator and Shannon diversity index quantified community richness and evenness, respectively. While species richness remained comparable between cohorts (Control: 800±100; NDI: 850±250; P=*0.58*), Shannon diversity declined significantly in diseased animals (7±2 versus 5±2, P<0.05) (Fig. 2A-B). Principal coordinate analysis revealed distinct clustering patterns between groups (*PERMANOVA:* $R^2$*=0.187,* P=0.001) (Fig. 2C).

Genus-level co-occurrence network mapping illuminated structural reorganization of the gut microbial ecosystem. Within the NDI cohort, several Firmicutes genera- including *Faecalibaculum*, *Limosilactobacillus*, and *Ligilactobacillus*-exhibited diminished abundance and reduced network connectivity. Conversely, Bacteroidetes members (Bacteroides, Muribaculum, Alloprevotella) expanded significantly. Notably, beneficial commensal interaction networks fragmented in diseased mice, coinciding with emergence of pathogen-enriched synergistic clusters-hallmarks of dysbiotic destabilization (Fig. 2D). Linear discriminant analysis effect size (*LEfSe; LDA threshold >3.0,* P<0.001) pinpointed taxonomic drivers of this dysbiosis: Prevotellaceae, Enterobacteriaceae, and Bacteroides showed marked enrichment in NDI animals, whereas Allobaculum abundance contracted substantially (Fig. 2E-F). Functional metagenomic inference via PICRUSt2 uncovered elevated antibiotic resistance gene pathways ($log_2$ *fold-change=0.87, FDR=0.012*) (Fig. 2G). Machine learning classification through Random Forest modeling established Escherichia-Shigella relative abundance as the strongest predictor of behavioral phenotype ($R^2$*=0.285,* P<0.001) (Fig. 2H).

**Association between tryptophan metabolism dysregulation and gut microbiota in NDI mice:** Serum metabolite profiles showed clear separation between the NDI and control groups according to OPLS-DA (*OPLS-DA:* $R^2X$*=0.612,* $R^2Y$*=0.987,* $Q^2$*=0.854*) (Fig. 3A).

The volcano plot showed a total of 2,188 significantly differential metabolites in the serum of NDI mice, with 1,204 significantly upregulated and 984 significantly downregulated (*VIP≥1,* P<0.05) (Fig. 3B). Serum metabolites in NDI mice were predominantly classified as benzene derivatives, amino acids and metabolites, heterocyclic compounds, and organic acids (Fig. 3C).

To further investigate the potential differential metabolites, we performed a heatmap cluster analysis of the selected metabolites. Compared with the control group, the tryptophan metabolism pathway in NDI mice showed significant alterations, specifically manifested by markedly reduced levels of indolepyruvate ($log_2FC$*=-1.52, FDR=0.003*), 5-hydroxyindoleacetic acid ($log_2FC$*=-1.38, FDR=0.007*), and indoleacetic acid ($log_2FC$*=-1.67,*

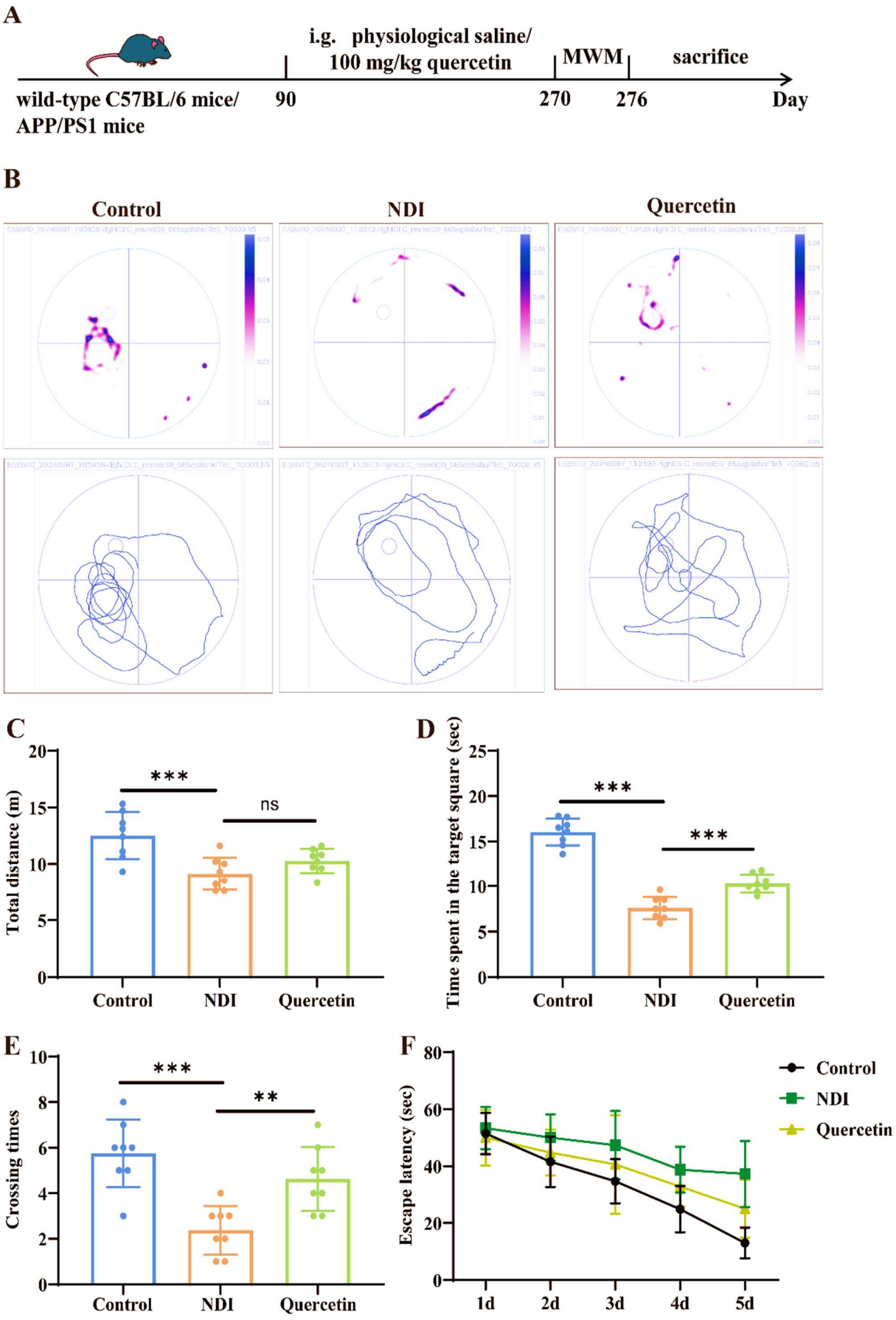


**Fig. 1:** Quercetin ameliorated cognitive impairment in NDI mice.

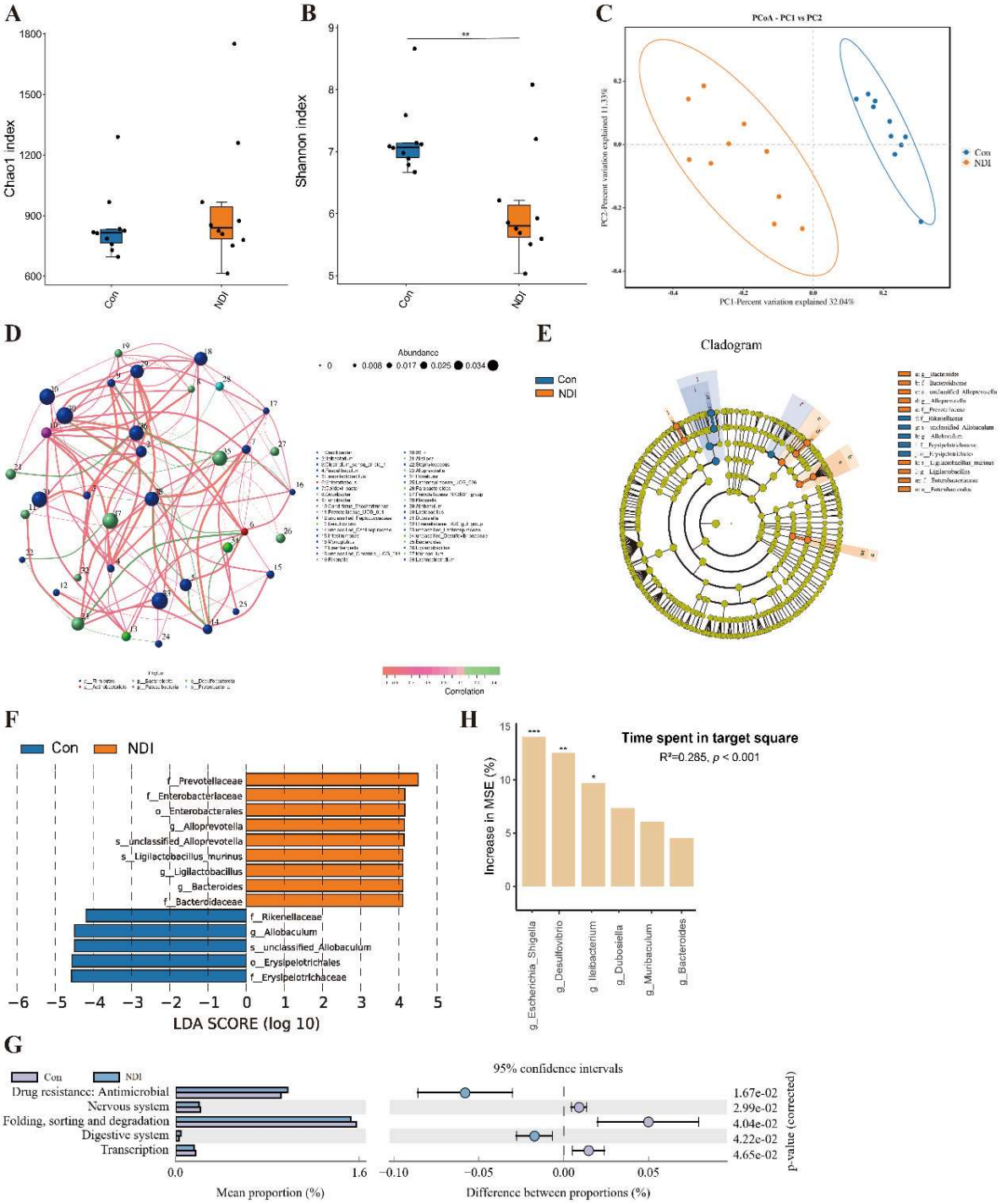


**Fig. 2:** Gut microbiota alterations associated with cognitive deficits in NDI mice. (A-B) α-diversity assessed by Chao1 (A) and Shannon (B) indices (n=10/group). (C) PCoA plot based on Bray-Curtis distances showing microbial community separation. (D) Genus-level co-occurrence networks comparing control and NDI groups. Node size indicates relative abundance; node color represents phylum assignment. Edge thickness corresponds to correlation strength; pink and green edges represent positive and negative correlations, respectively. (E-F) LEfSe analysis identifying differentially abundant taxa between groups. (G) Functional pathway predictions distinguishing control and NDI microbiomes. (H) Random forest model showing predictive value of dominant genera (>5% abundance) for NDI behavioral outcomes. Variable importance measured by MSE% increase; greater values denote higher predictive power. *P<0.05, **P<0.01, ***P<0.001.

*FDR=0.001*) (Fig. 3D). KEGG pathway enrichment analysis further confirmed that tryptophan metabolism (*enrichment ratio=4.32, FDR=0.002*) was one of the most significantly affected pathways (Fig. 3E). Tryptophan-derived metabolites serve as critical mediators of microbiota-host crosstalk, influencing intestinal homeostasis and systemic immune responses through multiple receptor-dependent mechanisms (Agus *et al.*, 2018). Spearman correlation revealed *Escherichia shigella* was positively correlated with tryptophan (*r=0.62,* P<0.01), indole-3-propionic acid (*r=0.68,* P<0.001), and the IPA/TRP ratio (*r=0.71,* P<0.001) (Fig. 3F).

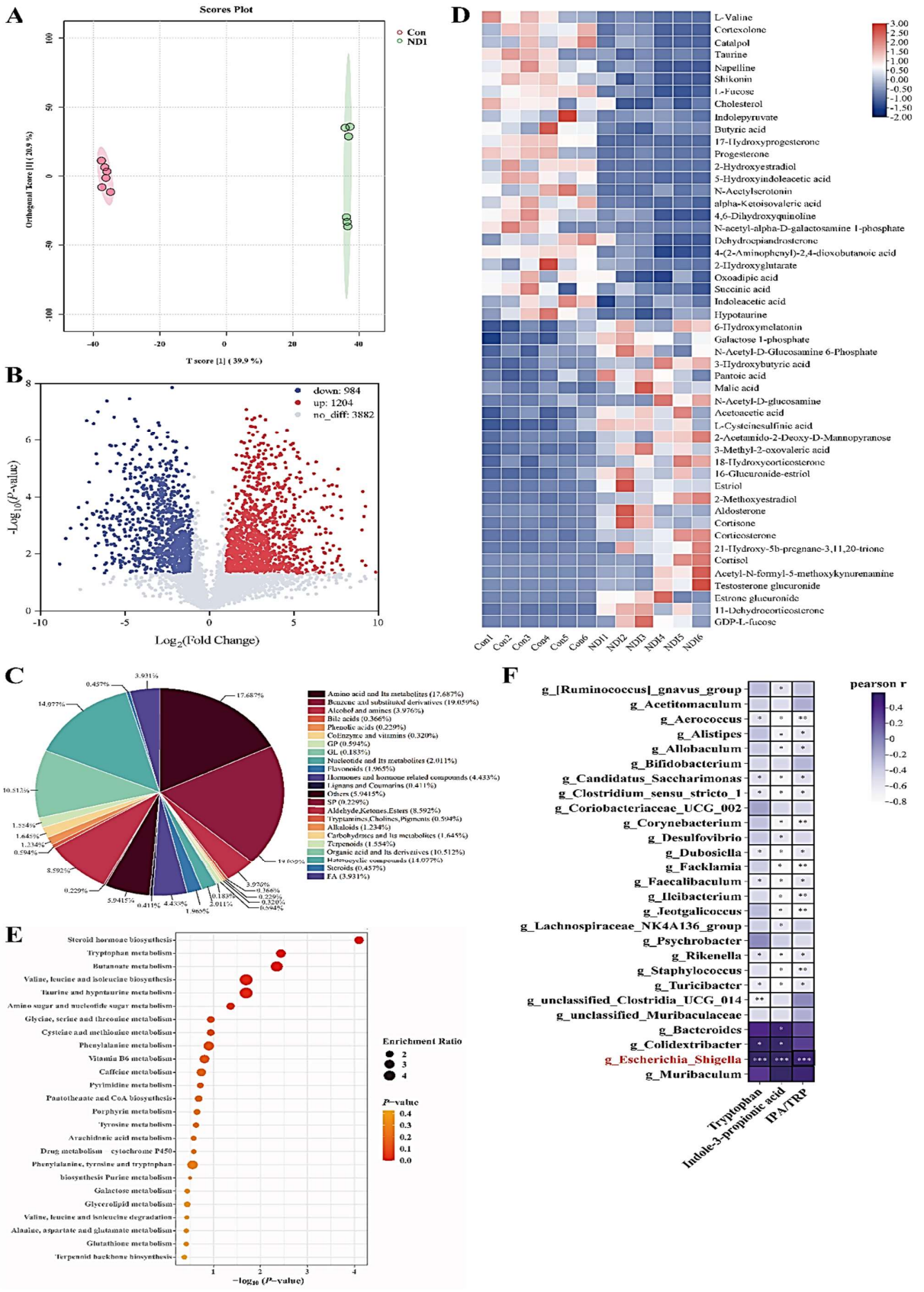


**Fig. 3:** Association between tryptophan metabolism dysregulation and gut microbiota in NDI mice. OPLS-DA score plot comparing serum metabolomes of NDI and control mice (n=10/group). (B) Volcano plot displaying differentially abundant metabolites. (C) Pie chart illustrating metabolite class distribution in NDI serum. (D) Heatmap depicting the top 50 metabolites across groups. (E) KEGG enrichment of altered metabolic pathways. (F) Spearman correlations between gut bacteria and tryptophan metabolites; darker purple indicates positive associations, lighter purple indicates negative associations. *P<0.05, **P<0.01, ***P<0.001.

**Quercetin reshaped the gut microbiota and corrected metabolic disruptions in NDI mice:** We next investigated whether quercetin's cognitive benefits involve gut microbiome restructuring through 16S rRNA sequencing. Rarefaction curves approached saturation, suggesting adequate sampling depth for community richness assessment (Fig. 4A). However, alpha-diversity metrics (Chao1 and Simpson indices) remained statistically equivalent across treatment groups (Fig. 4B-C). In contrast, principal coordinate analysis uncovered marked compositional divergence: quercetin intervention repositioned the microbial landscape from the disease state toward wild-type architecture (*PERMANOVA: $R^2$=0.142,* P=0.008; Fig. 4D). Taxonomic dissection at genus resolution identified selective bacterial modulation-quercetin suppressed disease-enriched Escherichia-Shigella (*$log_2FC$=-1.47, FDR=0.002*) and Bacteroides (*$log_2FC$=-0.89, FDR=0.021*) while amplifying Allobaculum (*$log_2FC$=1.68, FDR=0.008*). Other taxa such as Lactobacillus displayed non-significant directional changes (Fig. 4E). Paralleling these microbiome alterations, serum metabolome architecture shifted toward control-like profiles (*PERMANOVA: $R^2$=0.156, p=0.001*; Fig. 4F). Orthogonal HPLC quantification validated quercetin's capacity to partially restore tryptophan catabolism: circulating TRP concentrations increased 26% relative to untreated NDI mice (480±88 versus 380±86ng/mL, P<0.01), while the microbial metabolite IPA nearly doubled (1098±83 versus 579±99ng/mL, P<0.001) (Fig. 4G-H).

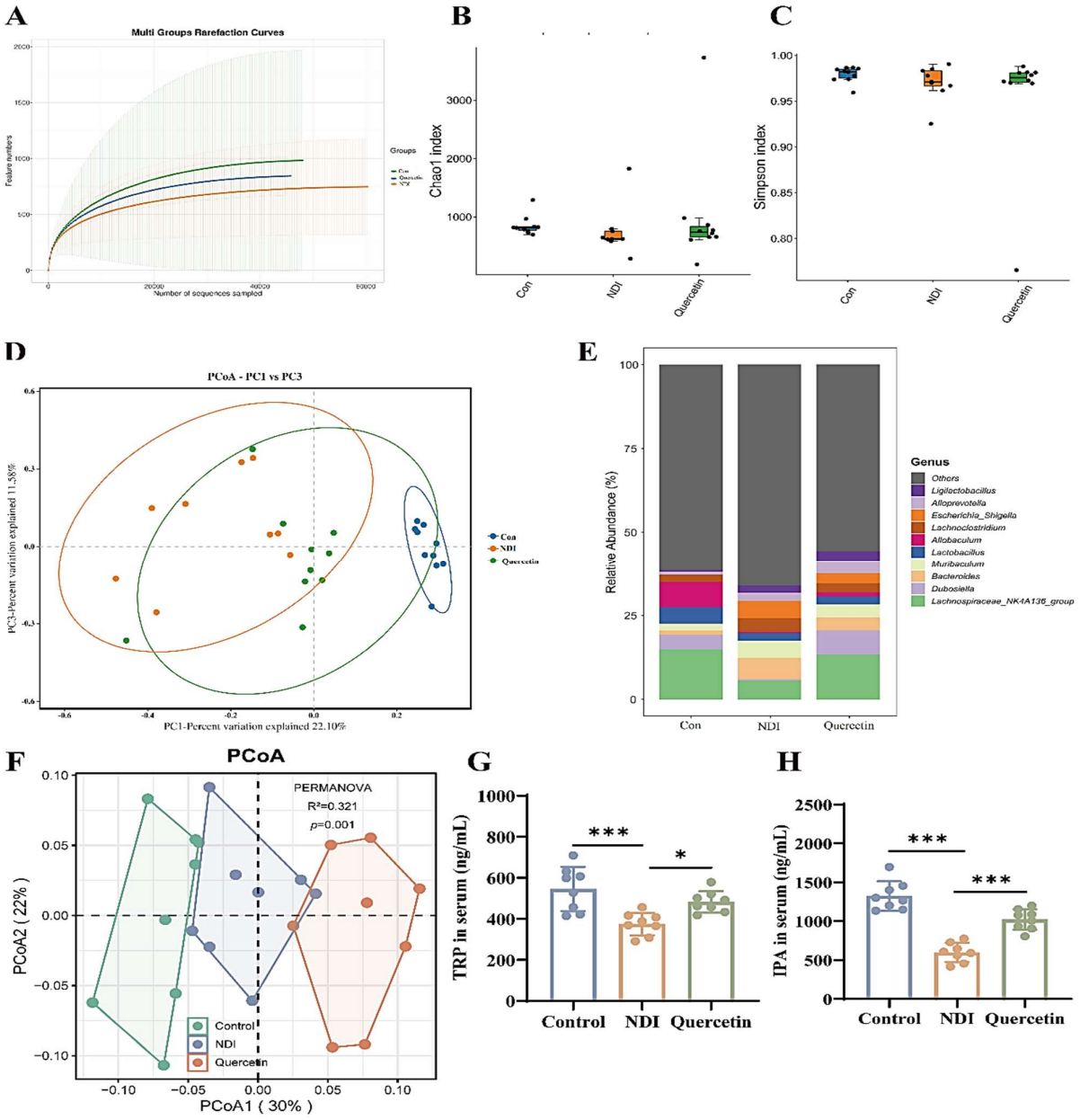


**Fig. 4:** Quercetin reshaped the gut microbiota and corrected metabolic disruptions in NDI mice. Rarefaction curves illustrating microbial species richness (n=10/group). (B-C) α-diversity measured by Chao1 (B) and Simpson (C) indices. (D) PCoA based on Bray-Curtis distances revealing bacterial community structure. (E) Genus-level taxonomic composition. (F) PCoA of serum metabolomes using Bray-Curtis distances (PERMANOVA, Adonis test). (G-H) Serum concentrations of TRP (G) and IPA (H). *P<0.05, ***P<0.001.

**Quercetin alleviated NDI cognitive impairment by activating the AhR pathway:** Cluster analysis integrating proteomics and metabolomics revealed that quercetin treatment significantly reshaped the systemic molecular expression profiles of NDI mice (Fig. 5A). KEGG pathway enrichment analysis revealed that tryptophan metabolism was identified as one of the most significantly enriched pathways affected by quercetin treatment in NDI mice (Fig. 5B). GSEA demonstrated that quercetin markedly upregulated the AhR signaling pathway *(NES=1.54,* P=0.01*)*, while showing no significant impact on NOD-like receptor signaling *(NES=0.97,* P=0.57*)* (Fig. 5C-D). Functional enrichment analysis of differentially expressed genes showed that the *AhR signaling pathway* was significantly downregulated in the NDI model, while quercetin treatment reversed this trend (Fig. 5E-F).

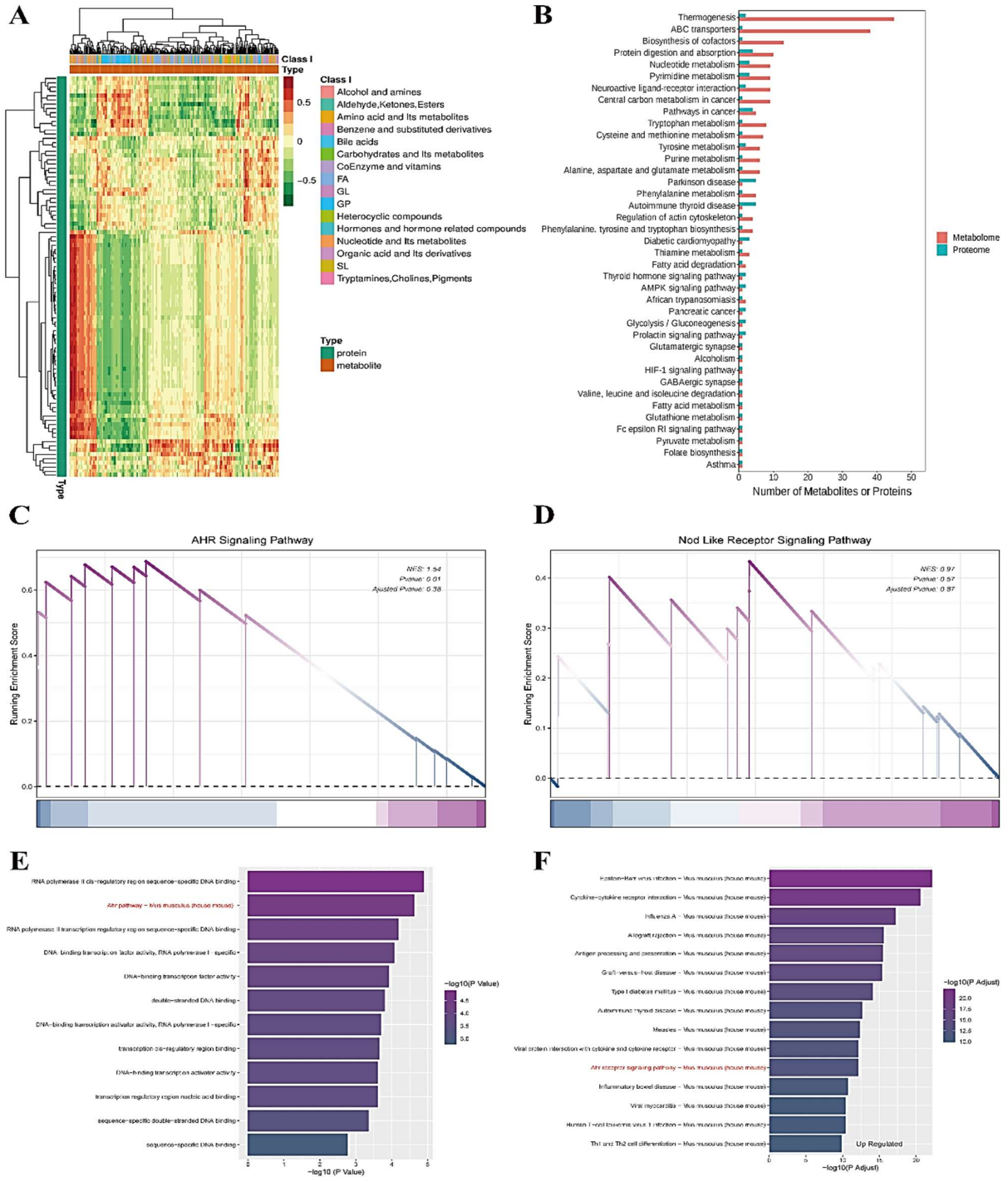


**Fig. 5:** Quercetin upregulated the AhR signaling pathway. (A) Heatmap clustering of differential metabolites and proteins (n=10/group). (B) KEGG pathway analysis for differentially expressed metabolites and proteins. (C-D) GSEA plot showing the enrichment signaling pathway associated with AhR (C) (*NES=1.54,* P=0.01), and *NOD-like receptor signaling pathway* (D) (*NES=0.97,* P=0.57). (E) Functional enrichment analysis indicated a downregulation of the *AhR signaling pathway* in the NDI model. (F) Functional enrichment analysis showed a significant upregulation of the *AhR signaling pathway* in response to quercetin treatment.

## DISCUSSION

Our study suggests that quercetin mitigates cognitive decline in APP/PS1 mice, likely by rebalancing the gut microbiota and restoring tryptophan metabolism. While our multi-omics approach points toward AhR pathway engagement, we interpret the causal links with caution.

The "microbiota-gut-brain axis" is increasingly recognized as a window into preclinical pathological processes, offering new avenues for early, noninvasive diagnosis of NDs (Jia *et al.*, 2025). Within our APP/PS1 model, microbial diversity contracted substantially alongside a distorted Firmicutes-to-Bacteroidetes ratio-phenotypes recapitulating dysbiotic signatures documented in human Alzheimer's cohorts and cognitively impaired aging canines (Zhuang *et al.*, 2018; Templeton *et al.*, 2023). Enterobacteriaceae and Bacteroides expansion echoed taxonomic shifts consistently reported across diverse neurodegenerative disorders (Kowalski and Mulak, 2019). Importantly, network topology analysis extended beyond mere compositional cataloging to reveal ecosystem-level instability: beneficial commensal interactions fragmented while opportunistic pathogen-associated taxa proliferated and established novel synergistic linkages.

The identification of *Escherichia shigella* abundance as a robust behavioral predictor ($R^2$*=0.285*) reinforces the hypothesis linking this genus to neuroinflammation, potentially via LPS-mediated pathways (Cattaneo *et al.*, 2017). However, establishing definitive causality requires validation through germ-free or antibiotic-depletion models, as host factors—such as intestinal barrier leakage or systemic immune deficits—could plausibly drive both microbial overgrowth and cognitive decline.

Regarding metabolic profiling, tryptophan pathway disruption characterized the NDI phenotype, aligning with clinical evidence positioning tryptophan catabolites as AD biomarkers (Vogt *et al.*, 2017). The strong correlation between *Escherichia shigella* and tryptophan/IPA levels (*r=0.62–0.71*) implies potential bacterial interference with substrate metabolism. Alternatively, host metabolic stress might create a selective niche for *Escherichia shigella*, or systemic inflammation could independently impact both microbiota and tryptophan catabolism (Dodd *et al.*, 2017). Consistent with its neuroprotective role, IPA was markedly reduced in NDI mice, corroborating reports linking diminished IPA production to cognitive impairment (Rothhammer *et al.*, 2016). Mechanistically, IPA and other microbial tryptophan metabolites limit CNS inflammation by activating AhR in astrocytes, thereby suppressing NF-κB-driven inflammatory programs (Rothhammer *et al.*, 2016). Although competitive tryptophan consumption by *Escherichia shigella* is a plausible mechanism, confirming bacterial utilization patterns necessitates future isotope tracing or culture-based studies.

Quercetin treatment shifted the microbial composition toward the control profile (*PERMANOVA R2=0.142*) and increased IPA levels by nearly 90%. This partial, rather than complete, restoration is characteristic of dietary polyphenols, which often exert selective modulation (Chen *et al.*, 2020; Rodríguez-Daza *et al.*, 2020). The specific suppression of *Escherichia shigella* and *Bacteroides,* alongside Allobaculum enrichment, likely reflects differential quercetin biotransformation capacities (Duda-Chodak *et al.*, 2015). Notably, the lack of significant *Lactobacillus* changes contrasts with some probiotic studies (Ma *et al.*, 2025), a discrepancy potentially attributable to variations in dosage, duration, or baseline microbiome states. Similar selective modulation has been observed with other dietary polyphenols, such as resveratrol, which reshapes gut microbiota composition to influence host metabolic pathways including bile acid metabolism (Chen *et al.*, 2016). The translational potential of these findings for companion animal cognitive dysfunction warrants further investigation.

Mechanistically, GSEA analysis demonstrated *AhR pathway* upregulation (*NES=1.54, p=0.01*) following quercetin treatment. While IPA is an established AhR agonist (Hubbard *et al.*, 2015), our study lacks direct validation of AhR protein activation (e.g., nuclear translocation, target gene qPCR). Furthermore, quercetin can directly activate AhR independent of microbial metabolites (Ciolino *et al.*, 1999), complicating attribution of pathway activation solely to gut-brain axis mechanisms. The absence of *NOD-like receptor pathway* changes (*NES=0.97,* P=0.57) suggests pathway specificity, though this does not exclude involvement of other inflammatory cascades. Recent studies demonstrate AhR activation suppresses microglial *NF-κB signaling* and *neuroinflammation* (Rothhammer *et al.*, 2018), but whether this mechanism mediates quercetin's cognitive benefits in our model requires validation using AhR antagonists or knockout mice.

Several constraints should be acknowledged. First, 16S rRNA sequencing provides genus-level resolution but cannot identify IPA-producing species. Shotgun metagenomics and functional gene profiling would enable mechanistic insights into bacterial tryptophan metabolism. Second, the absence of fecal microbiota transplantation experiments limits causal inference regarding microbiota contributions to cognitive phenotypes. Third, we did not measure intestinal barrier integrity (e.g., zonulin, LPS translocation) or neuroinflammatory markers, which are critical gut-brain axis mediators (Cryan *et al.*, 2019). Finally, exclusive use of male mice precludes generalization, as sex differences in microbiota-brain interactions are increasingly recognized.

Our findings support quercetin as a candidate microbiota-targeted intervention for neurodegenerative diseases, with potential applications in both human medicine and veterinary neurology. The partial restoration of gut homeostasis suggests combination strategies, as quercetin plus probiotics or prebiotics, may enhance therapeutic efficacy, as demonstrated in recent clinical trials for mild cognitive impairment. Translation to companion animals with cognitive dysfunction syndrome requires dose optimization and safety evaluation in veterinary populations.

In conclusion, quercetin ameliorates cognitive deficits in APP/PS1 mice through mechanisms that appear to involve gut microbiota remodeling and tryptophan metabolism restoration, with potential AhR pathway engagement. However, the causal contributions of these pathways require validation through targeted genetic and pharmacological approaches. These findings provide a foundation for developing microbiota-based interventions for neurodegenerative diseases across species.

**Funding:** This work is supported by a grant from the Shandong Second Medical University 2024 Affiliated Hospitals (Teaching Hospitals) Research and Development Fund Project（No. 2024FYM014, China), Weifang Chinese Medicine Science and Technology Research Program（No. WFZYY2024-4-093, China) and Weifang Young Medical Talent Support Project Subsidies.

**Ethical approval of the study:** All experimental protocols in this study received formal approval from the Laboratory Animal Ethics Committee of Shandong Second Medical University. This ethical review is essential to guarantee compliance with animal welfare regulations and ethical standards for animal experimentation. All operations were conducted in accordance with the Guide for the Care and Use of Laboratory Animals.

**Authors contribution:** Ying Feng and Yan hua Shi contributed equally to this work. Xinjun Yu conceptualized the study, supervised the project, and acquired funding. Methodology was developed by Ying Feng, Yan hua Shi, and Tao Wang. Investigation was carried out by Ying Feng, Yan hua Shi, Jin yang Han, Dan dan Li, Xiao tong Zhang, and Qian Xu. Formal analysis was performed by Tao Wang and Jin yang Han. Ying Feng and Yan hua Shi wrote the original draft, which was subsequently reviewed and edited by Xinjun Yu and Tao Wang.

## REFERENCES

Abou Izzeddine N, Ahmad K, Bacha C, *et al.*, 2025. The microbial guardians: Unveiling the role of gut microbiota in shaping neurodegenerative disease. IBRO Neurosci Rep 19:17-37.

Agus A, Planchais J and Sokol H, 2018. Gut microbiota regulation of tryptophan metabolism in health and disease. Cell Host Microbe 23(6):716-724.

Anders S and Huber W, 2010. Differential expression analysis for sequence count data. Genome Biol 11(10):R106.

Bolyen ERideout JR, Dillon MR, *et al.*, 2019. Reproducible, interactive, scalable and extensible microbiome data science using QIIME 2. Nat Biotechnol 37(8):852-857.

Bromley-Brits K, Deng Y and Song W, 2011. Morris water maze test for learning and memory deficits in Alzheimer's disease model mice. J Vis Exp (53).

Callahan BJ, McMurdie PJ, Rosen MJ, *et al.*, 2016. DADA2: High-resolution sample inference from Illumina amplicon data. Nat Methods 13(7):581-583.

Cattaneo A, Cattane N, Galluzzi S, *et al.*, 2017. Association of brain amyloidosis with pro-inflammatory gut bacterial taxa and peripheral inflammation markers in cognitively impaired elderly. Neurobiol Aging 49:60-68.

Chen M, Xiao D, Liu W, *et al.*, 2020. Intake of Ganoderma lucidum polysaccharides reverses the disturbed gut microbiota and metabolism in type 2 diabetic rats. Int J Biol Macromol 155:890-902.

Chen ML, Yi L, Zhang Y, *et al.*, 2016. Resveratrol attenuates Trimethylamine-N-Oxide (TMAO)-Induced atherosclerosis by regulating TMAO synthesis and bile acid metabolism via remodeling of the gut microbiota. mBio 7(2):e02210-02215.

Chong J, Wishart DS and Xia J, 2019. Using MetaboAnalyst 4.0 for comprehensive and integrative metabolomics data analysis. Curr Protoc Bioinformatics 68(1):e86.

Ciolino HP, Daschner PJ and Yeh GC, 1999. Dietary flavonols quercetin and kaempferol are ligands of the aryl hydrocarbon receptor that affect CYP1A1 transcription differentially. Biochem J 340 ( Pt 3)(Pt 3):715-722.

Cox J, Hein MY, Luber CA, *et al.*, 2014. Accurate proteome-wide label-free quantification by delayed normalization and maximal peptide ratio extraction, termed MaxLFQ. Mol Cell Proteomics 13(9):2513-2526.

Cox J and Mann M, 2008. MaxQuant enables high peptide identification rates, individualized p.p.b.-range mass accuracies and proteome-wide protein quantification. Nat Biotechnol 26(12):1367-1372.

Cryan JF, O'Riordan KJ, Cowan CSM, *et al.*, 2019. The microbiota-gut-brain axis. Physiol Rev 99(4):1877-2013.

Dewey CW, 2025. Poop for thought: Can fecal microbiome transplantation improve cognitive function in aging dogs? Open Vet J 15(2):556-564.

Dodd D, Spitzer MH, Van Treuren W, *et al.*, 2017. A gut bacterial pathway metabolizes aromatic amino acids into nine circulating metabolites. Nature 551(7682):648-652.

Duda-Chodak A, Tarko T, Satora P, *et al.*, 2015. Interaction of dietary compounds, especially polyphenols, with the intestinal microbiota: a review. Eur J Nutr 54(3):325-341.

Dunn WB, Broadhurst D, Begley P, *et al.*, 2011. Procedures for large-scale metabolic profiling of serum and plasma using gas chromatography and liquid chromatography coupled to mass spectrometry. Nat Protoc 6(7):1060-1083.

Hubbard TD, Murray IA and Perdew GH, 2015. Indole and Tryptophan Metabolism: Endogenous and Dietary Routes to Ah Receptor Activation. Drug Metab Dispos 43(10):1522-1535.

Jankowsky JL, Fadale DJ, Anderson J, *et al.*, 2004. Mutant presenilins specifically elevate the levels of the 42 residue beta-amyloid peptide in vivo: evidence for augmentation of a 42-specific gamma secretase. Hum Mol Genet 13(2):159-170.

Jia L, Ke Y, Zhao S, *et al.*, 2025. Metagenomic analysis characterizes stage-specific gut microbiota in Alzheimer's disease. Mol Psychiatry 30(9):3951-3962.

Jung JH, Kim G, Byun MS, *et al.*, 2022. Gut microbiome alterations in preclinical Alzheimer's disease. PLoS One 17(11):e0278276.

Kowalski K and Mulak A, 2019. Brain-Gut-Microbiota Axis in Alzheimer's Disease. J Neurogastroenterol Motil 25(1):48-60.

Liu J, Liu Y, Huang C, *et al.*, 2025. Quercetin-Driven Akkermansia Muciniphila Alleviates Obesity by Modulating Bile Acid Metabolism via an ILA/m(6)A/CYP8B1 Signaling. Adv Sci (Weinh) 12(12):e2412865.

Love MI, Huber W and Anders S, 2014. Moderated estimation of fold change and dispersion for RNA-seq data with DESeq2. Genome Biol 15(12):550.

Lu Y, Zamora-Ros R, Chan S, *et al.*, 2017. Dietary polyphenols in the aetiology of crohn's disease and ulcerative colitis-a multicenter european prospective cohort study (EPIC). Inflamm Bowel Dis 23(12):2072-2082.

Lv M, Yang S, Cai L, *et al.*, 2018. Effects of Quercetin Intervention on Cognition Function in APP/PS1 Mice was Affected by Vitamin D Status. Mol Nutr Food Res 62(24):e1800621.

Ma M, Li B, Qu Z, *et al.*, 2025. Efficacy of probiotics in patients with cognitive impairment: A systematic review and meta-analysis. PLoS One 20(5):e0321567.

McMillan JR, Armstrong PM and Andreadis TG, 2020. Patterns of mosquito and arbovirus community composition and ecological indexes of arboviral risk in the northeast United States. PLoS Negl Trop Dis 14(2):e0008066.

Metwally E, Al-Abbadi HA, Hussain T, *et al.*, 2023. Calpain signaling: from biology to therapeutic opportunities in neurodegenerative disorders. Front Vet Sci 10:1235163.

Porras D, Nistal E, Martínez-Flórez S, *et al.*, 2017. Protective effect of quercetin on high-fat diet-induced non-alcoholic fatty liver disease in mice is mediated by modulating intestinal microbiota imbalance and related gut-liver axis activation. Free Radic Biol Med 102:188-202.

Quast C, Pruesse E, Yilmaz P, *et al.*, 2013. The SILVA ribosomal RNA gene database project: improved data processing and web-based tools. Nucleic Acids Res 41(Database issue):D590-596.

Rodríguez-Daza MC, Roquim M, Dudonné S, *et al.*, 2020. Berry polyphenols and fibers modulate distinct microbial metabolic functions and gut microbiota enterotype-like clustering in obese mice. Front Microbiol 11:2032.

Rothhammer V, Borucki DM, Tjon EC, *et al.*, 2018. Microglial control of astrocytes in response to microbial metabolites. Nature 557(7707):724-728.

Rothhammer V, Mascanfroni ID, Bunse, L *et al.*, 2016. Type I interferons and microbial metabolites of tryptophan modulate astrocyte activity and central nervous system inflammation via the aryl hydrocarbon receptor. Nat Med 22(6):586-597.

Rothhammer V and Quintana FJ, 2019. The aryl hydrocarbon receptor: an environmental sensor integrating immune responses in health and disease. Nat Rev Immunol 19(3):184-197.

Sampson TR, Debelius JW, Thron T, *et al*., 2016. Gut microbiota regulate motor deficits and neuroinflammation in a model of Parkinson's Disease. Cell 167(6):1469-1480.e1412.

Smith CA, Want EJ, O'Maille G, *et al*., 2006. XCMS: processing mass spectrometry data for metabolite profiling using nonlinear peak alignment, matching, and identification. Anal Chem 78(3):779-787.

Story BD, Miller ME, Bradbury AM, *et al*., 2020. Canine models of inherited musculoskeletal and neurodegenerative diseases. Front Vet Sci 7:80.

Sun J, Zhang Y, Kong Y, *et al*., 2022. Microbiota-derived metabolite Indoles induced aryl hydrocarbon receptor activation and inhibited neuroinflammation in APP/PS1 mice. Brain Behav Immun 106:76-88.

Templeton GB, Fefer G, Case BC, *et al*., 2023. Longitudinal analysis of canine oral microbiome using whole genome sequencing in aging companion dogs. Animals (Basel) 13(24)

Tyanova S, Temu T, Sinitcyn P, *et al*., 2016. The Perseus computational platform for comprehensive analysis of (prote)omics data. Nat Methods 13(9):731-740.

Vogt NM, Kerby RL, Dill-McFarland KA, *et al*., 2017. Gut microbiome alterations in Alzheimer's disease. Sci Rep 7(1):13537.

Vorhees CV and Williams MT, 2006. Morris water maze: procedures for assessing spatial and related forms of learning and memory. Nat Protoc 1(2):848-858.

Wihadmadyatami H, Zulfikar MA, Herawati H, *et al*., 2025. Neuroprotection effect of bovine umbilical mesenchymal stem cell-conditioned medium on the rat model of Alzheimer's disease mediated by upregulation of BDNF and NGF and downregulation of TNF-α and IL-1β. Open Vet J 15(1):151-161.

Wiśniewski JR, Zougman A, Nagaraj N, *et al*., 2009. Universal sample preparation method for proteome analysis. Nat Methods 6(5):359-362.

Yu G, Wang LG, Han Y, *et al*., 2012. clusterProfiler: an R package for comparing biological themes among gene clusters. Omics 16(5):284-287.

Zhuang ZQ, Shen LL, Li WW, *et al*., 2018. Gut Microbiota is Altered in Patients with Alzheimer's Disease. J Alzheimers Dis 63:1337-1346.